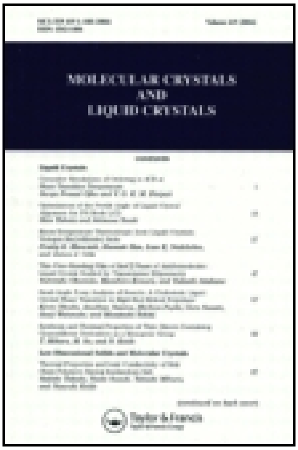

Molecular Crystals and Liquid Crystals
Publication details, including instructions for authors and subscription information:
http://www.tandfonline.com/loi/gmcl20

TRANSIENT DIRECTOR ORIENTATION PATTERN OF CREEPING PLANE POISEUILLE FLOW OF A NEMATIC POLYMER

W. H. Han [a] , S. T. Koh [a] , S. G. Noh [a] , J. K. Jeon [a] & J. H. Cho [a]

[a] Department of Chemical Engineering, Dong Yang University, Kyochondong 1-bunjee, Young Jou City, Kyungbook 750-711, Korea

Version of record first published: 07 Jan 2010

To cite this article: W. H. Han, S. T. Koh, S. G. Noh, J. K. Jeon & J. H. Cho (2004): TRANSIENT DIRECTOR ORIENTATION PATTERN OF CREEPING PLANE POISEUILLE FLOW OF A NEMATIC POLYMER, Molecular Crystals and Liquid Crystals, 413:1, 355-362

To link to this article: http://dx.doi.org/10.1080/15421400490437015

Mol. Cryst. Liq. Cryst., Vol. 413, pp. 355/[2491]–362/[2498], 2004

ISSN: 1542-1406 print/1563-5287 online
DOI: 10.1080/15421400490437015

TRANSIENT DIRECTOR ORIENTATION PATTERN OF CREEPING PLANE POISEUILLE FLOW OF A NEMATIC POLYMER

W. H. Han, S. T. Koh, S. G. Noh, J. K. Jeon, and J. H. Cho
Department of Chemical Engineering, Dong Yang University
Kyochondong 1-bunjee, Young Jou City, Kyungbook 750-711, Korea

The time-dependent Leslie-Ericksen equation in numerically solved for creeping plane poiseuille flow of a nematic polymer (Poly Benzyl Glutamate). The Leslie coefficients and Frank orientation curvature elasticity constants of the nematic polymer reported in the literature were used for the computations of three dimensional director time (t) evolution over the two-dimensional (x-y) plane. The flow is along the x-axis, and the thickness axis the y-axis. On the bounding plates assumed strong homeotropic anchoring condition. On the inlet and outlet flow boundaries, zero surface couple condition is used.

Although poiseuille flow has a zero shearing line in the middle with changing sing of shear rate when going through the mid gap region, unlike simple shear flow, directors escape the shear (x-y) plane as flow rate increases, which this computation study shows in accordance with various experimental studies. As the center velocity (U) increases, complex 3-D orientation structure emerges. When U is further increased, tube orientation walls reminiscent of the tube walls of shear flow emerges, not through pinching and reconnection of orientation wall pair, but through emanation from the central backbone orientation wall structure.

Keywords: Leslie-Ericksen theory; nematodynamics; pattern formation; poiseuille flow; polymeric liquid crystals

INTRODUCTION

Poiseuille flow is a very important flow phenomenon in liquid crystal processing. Unlike shear flow, poiseuille flow has a zero shear rate zone in the gap middle where viscous torque vanishes. For flow non-aligning nematics like polymeric liquid crystals, it is very common to observe banded texture seen through polarizing microscope when the sample

Address correspondence to W. H. Han, Department of Chemical Engineering, Dong Yang University, Kyochondong 1-bunjee, Young Jou City, Kyungbook 750-711, Korea.

experience flow deformation [1–3]. There have been numerous experimental evidence of out-of-shear plane orientation during flow of non-aligning nematics. This necessitates fully three-dimensional orientation approach like the present study.

This study presents a nonlinear numerical analysis of the Leslie-Ericksen equation on poiseuille flow using the finite element method. Material constants for the Leslie-Ericksen theory has been taken from the literature [4]. The computed results are presented with scientific visualization method.

THEORY AND SOLUTION METHOD

The Leslie-Ericksen (L-E) theory consists of the linear momentum balance and the torque balance of the unit vector **n**, director, representing the local orientation [5]. The linear momentum balance is given by:

$$\rho v = \mathbf{f} + \nabla \cdot \boldsymbol{\sigma} \tag{1}$$

where ρ, v, $\mathbf{f}$ and $\boldsymbol{\sigma}$ are the density, velocity, body force per unit volume and total stress, respectively. The superposed dot denotes the material time derivative. The total stress tensor $\boldsymbol{\sigma}$ is given by

$$\boldsymbol{\sigma} = -p\delta - \frac{\boldsymbol{\partial} F}{(\partial \nabla \mathbf{n})^T} \cdot \nabla \mathbf{n} + \alpha_1(\mathbf{nn} : \mathbf{A})\mathbf{nn} + \alpha_2 \mathbf{nN} + \alpha_3 \mathbf{Nn} + \alpha_4 \mathbf{A} + \alpha_5 \mathbf{nn} \cdot \mathbf{A} + \alpha_6 \mathbf{A} \cdot \mathbf{nn} \tag{2}$$

where p, δ, α_i (i=1,. . .,6), $\mathbf{A}$ and $\mathbf{N}$ are the pressure, unit tensor, Leslie viscosity coefficients, rate of deformation tensor, and corrotational time derivative of $\mathbf{n}$, respectively. The rate of deformation tensor $\mathbf{A}$ and the corrotational time derivative of the director $\mathbf{N}$ are given by

$$2\mathbf{A} = (\nabla v + (\nabla v)^T), \quad \mathbf{N} = \dot{\mathbf{n}} - \omega \cdot \mathbf{n} \tag{3}$$

where the rate of rotation tensor $\boldsymbol{\omega}$ is

$$2\omega = (\nabla v - (\nabla v)^T). \tag{4}$$

The torque balance is given by

$$0 = \boldsymbol{\Gamma}^v + \boldsymbol{\Gamma}^e, \tag{5}$$

where the viscous torque $\boldsymbol{\Gamma}^v$ and the elastic torque $\boldsymbol{\Gamma}^e$ are given by:

$$\boldsymbol{\Gamma}^v = -\mathbf{n} \times (\gamma_1 \mathbf{N} + \gamma_2 \mathbf{A} \cdot \mathbf{n}), \tag{6}$$

$$\Gamma^e = -\mathbf{n} \times \left(\frac{\partial F}{\partial \mathbf{n}} - \nabla \cdot \frac{\partial F}{\partial (\nabla \mathbf{n})^T} \right) \tag{7}$$

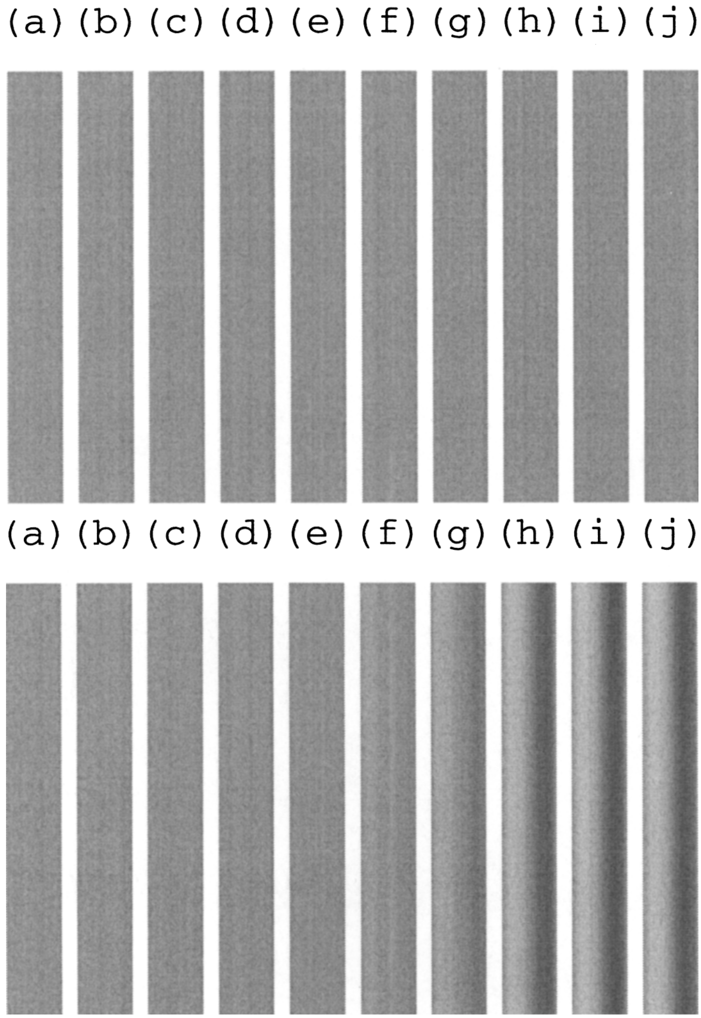

FIGURE 1 Texture evolutions of n_z(top row) and n_x(bottom row) for E = 70040. Each rectangle represents a director field at time t between two parallel plates normal to y-axis. Flow is upward and vertical. Black color means $n_i = -1$, white $n_i = +1$, medium gray $n_i = 0$. Time(sec) for each rectangle is: (a) 0.1, (b) 1.1, (c) 4.9, (d) 19.6, (e) 76, (f) 293, (g) 1125, (h) 3720, (i) 8800 and (j) 26000.

where γ_1 and γ_2 are the rotational and irrotational viscosities, respectively [10]. The Frank orientation curvature elastic energy F is given by:

$$2F = K_{11}(\nabla \cdot \mathbf{n})^2 + K_{22}(\mathbf{n} \cdot \nabla \times \mathbf{n})^2 + K_{33}|\mathbf{n} \times \nabla \times \mathbf{n}|^2 \tag{8}$$

where K_{11}, K_{22}, and K_{33} are the splay, twist and bend constants, respectively. The orientation behavior during flow is controlled by the Ericksen number E, a characteristic ratio between the viscous and elastic torques, given by

$$E = \gamma_1 hU / \left(\prod_{i=1}^{3} K_{ii} \right)^{1/3} \tag{9}$$

where U and $h(= 3.5 \times 10^{-4} m)$ denote the maximum center velocity and the gap thickness, respectively. The experimentally measured material constants are (γ_1, γ_2) = (6.938, –6.902) Pa·s and (K_{11}, K_{22}, K_{33} = (1.21, 0.078, 0.763) $\times 10^{-11}$ N [4].

The Galerkin finite element method and a fully implicit time integration method were used with 60 by 60 quadrilateral bilinear elements to obtain the director field, $\mathbf{n}$ = (n_x(x,y,t), n_y(x,y,t), n_z(x,y,t)) under simple poiseuille flow kinematics $\mathbf{v} = (U(h-y)y\Phi(t),0,0))$ where Φ is the Heavyside step function. The full detailed equations are found in [6]. At t = 0, uniform homeotorpic director field is randomly perturbed with a maximum perturbation $\delta n_i^2 = 10^{-4}, i = x, y, z$. The fixed homeotropic abchoring boundary condition is used ($\mathbf{n}$ = (0,1,0) at $y = 0$ and h). To minimize the inlet and outlet end effects of finite length computational domain, a large aspect ratio (length/thickness) of 16 was used. At the inlet and outlet, vanishing contact torque condition convenient for implementing finite element method was used.

RESULTS AND DISCUSSION

All the orientation textures computed in this study are presented in density plots, in which n_i ($i = x$, z) values are represented with gray scale; $n_i = +1$ is shown with white, $n_i = +1$ black, $n_i = 0$ medium gray.

Other inbetween numerical values of n_i are represented with shaded regions in such a way that regions with higher values are lighter.

Figure 1 shows that when $E < E_c$ ($E_c \approx 80,000$), the directors remain in the shear plane spanned by the flow axis (x) and the thickness axis (y). E_c, the critical Ericksen number, is defined as the Ericksen number (Eq. 9) for which directors can no longer be constrained within the shear plane (x-y plane) everywhere. Note the relatively large magnitude of E_c which is due to the fact that the thickness used in shear flow case does not correspond to the thickness of Poiseuille flow case; the effective thickness would be much smaller for the Poiseuille flow cell.

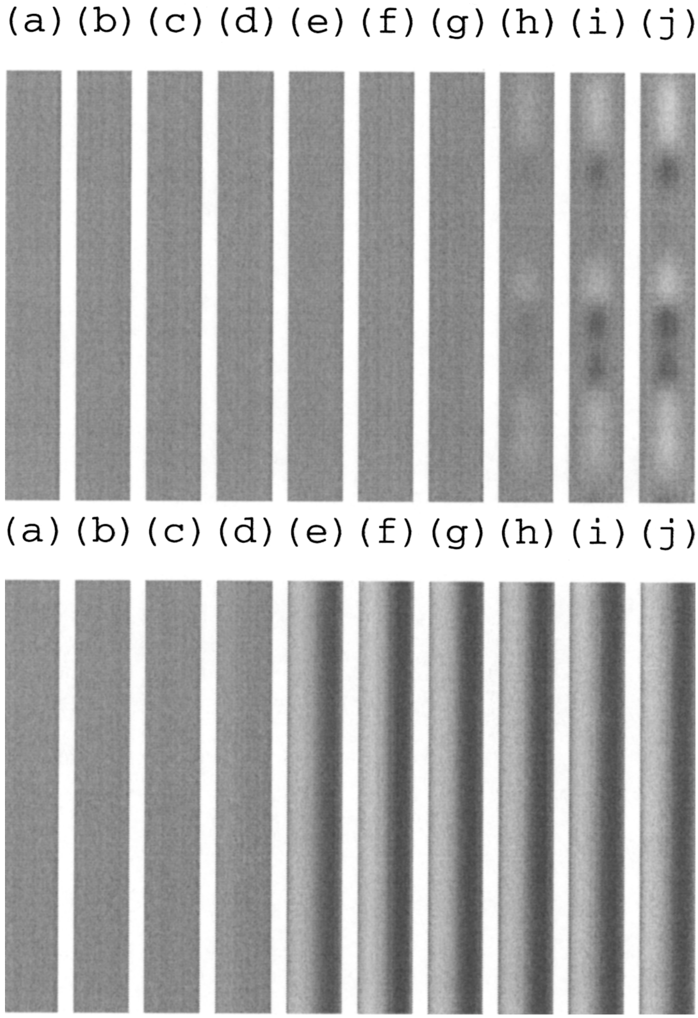

FIGURE 2 Texture evolutions of n_z(top) and n_x(bottom) for E = 81700. All the conventions used in this figure are the same as in the Figure 1. Time(sec) for each rectangle is: (a) 0.1, (b) 1.1, (c) 19.6, (d) 293, (e) 3285, (f) 19800, (g) 203700, (h) 1128000, (i) 1925000, (j) 2355000.

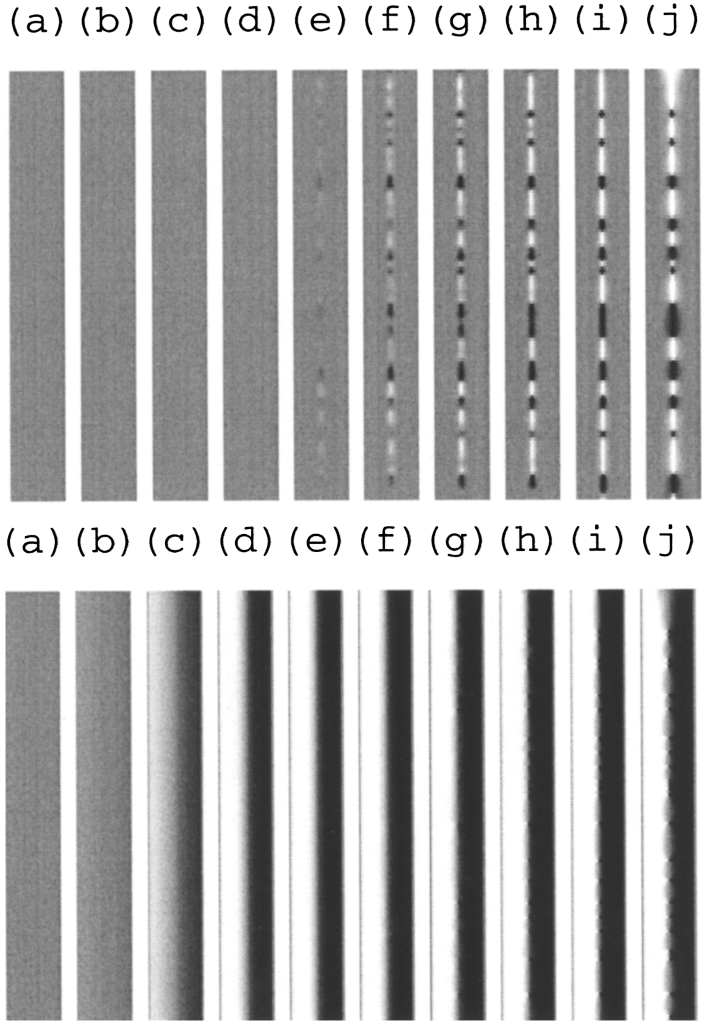

FIGURE 3 Texture evolutions of n_z(top) and n_x(bottom) for $E = 291{,}800$. All the conventions used in this figure are the same as in the Figure 1. Time(sec) for each rectangle is: (a) 0.1, (b) 9.9, (c) 95.7, (d) 496 (e) 1770, (f) 2320, (g) 2730, (h) 3130, (i) 3880, (j) 20800000.

When the upward flow starts the initial orientation is like Figure 1(a) where the monodomain texture with homeotropic anchoring ($n_x = 0$, $n_y = 1$, $n_z = 0$) is shown with medium gray color. Figure 1(j) corresponds to a steady state orientation texture in which the directors orient counter-clockwise in the lower (or left) half and clockwise in the upper (or right)

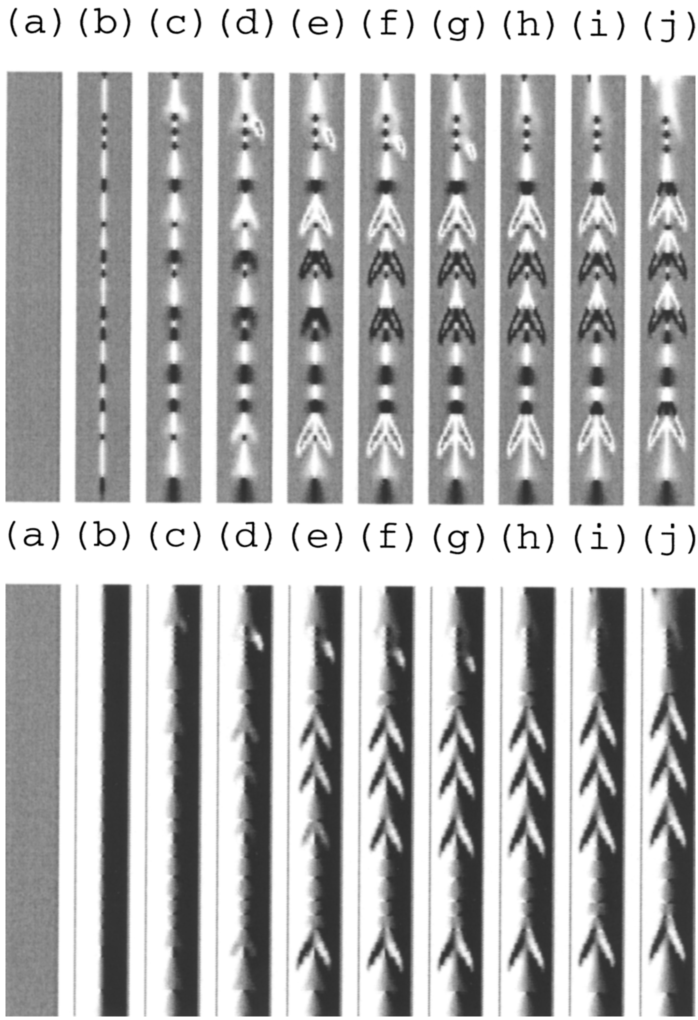

FIGURE 4 Texture evolutions of n_z and n_x for $E = 5.837 \times 10^8$. All the conventions used in this figure are the same as in the Figure 1. Time(sec) for each rectangle is: (a)0.1, (b)2532, (c)9609, (d)13607 (e)20676, (f) 25084, (g)27701, (h)42308, (i) 64226, (j)95669.

half within the shear plane. As $E > E_c$, Figure 2 shows that there are non-zero n_z regions building up represented by either darker or brighter region. The corresponding bottom n_x plot consists of composite of dark and bright bars, which means that the director is in one-way twist mode in the middle gap region. Figure 3 shows that when E further increases, the director field forms connected alternating orientation wall structure consisting of $n_z = \pm 1$ segments in the middle gap. n_x plot of Figure 3 shows wavy middle layer which signals some further structural transition. Figure 4 for higher flow rate shows a such a transition. Black and white orientation wall structure give birth to orientation tube walls from the backbone orientation wall. The backbone orientation wall is like a tree stem, and the orientation tube wall tree leaves. A pair of counter shear flows with opposite shear rate sign might form a similar structure with orientation tube walls of the same semi-axis orientation [7–8], but the middle zero shear rate zone of poiseuille flow produces tube walls connected which each other through the backbone orientation wall.

Since the ratio of length to thickness is 16:1 and the tube walls appeared four times along the flow axis (y), the period of the orientation tube walls is about four times the thickness on average. One notable feature of the computed herring-bone-like texture is that all the steady state tube walls are composed of black ($n_z = -1$) and white ($n_z = +1$) orientation walls. The herring-bone-like orientation texture shown in Figure 4(j) is at steady state, meaning that the texture is permanent and stable in Poiseuille flow.

CONSLUSIONS

A cascade of complex orientation texture evolutions during poiseuille flow has been computed using the literature values of the experimentally measured Leslie coefficients and Frank elastic constants. Unlike the shear flow computation results, orientation tube orientation walls were emanated from the backbone orientation wall running through the weak shear rate middle gap region. The computed herring-bone-like orientation wall structure might be a quite interesting topic for experimental study. A further study will shed more light on the basis uinderstanding of these computed phenomena.

REFERENCES

[1] Elliott, A. & Ambrose, E. J. (1950). *Discuss. Faraday Soc. 9*, 246.
[2] Toth, W. J. & Tobolsky, A. V. (1970). *Polymer Letters 8*, 537.
[3] Kiss, G. & Porter, R. S. (1980). *Mol. Cryst. Liq. Cryst.*, *60*, 267.
[4] Srajer, G., Fraden, S., & Meyer, R. B. (1989). *Phys. Rev. A 39*, 4828.
[5] de Gennes, P. G. & Prost, J. (1993). *The phsysics of liquid crystals*, Clarendon Press: Oxford.
[6] Han, W. H., Ph.D. (1995). Dissertation, McGill University.
[7] Han, W. H. & Rey, A. D. (1995). *Macromolecules 28*, 8401.
[8] Han, W. H., Cho, J. H., Jeon, J. K., Noh, S. G., & Koh, S. T. (2001). *Mol. Cryst. Liq. Cryst. 366*, 929.